Numerical Calculations on Reflection Processes of Ionizing Shocks on the End Wall of a Shock Tube

Yasunari Takano and Teruaki Akamatsu

Kyoto University, Kyoto, Japan

(Z. Naturforsch. **32 a**, 986–993 [1977]; received June 27, 1977)

Numerical calculations have been made about shock reflection processes in ionizing argon on the end wall of a shock tube. The two-step Lax-Wendroff scheme was employed to solve time-dependent one-dimensional inviscid flow problems for ionizing gases. Complicated flowfields were found to occur due to interactions between ionization relaxation processes and reflected shocks. Calculations were performed for three cases: incident-shock Mach number $M_s = 16$ and initial pressure $p_1 = 1$ torr; $M_s = 14$ and $p_1 = 3$ torr; $M_s = 12$ and $p_1 = 5$ torr.

1. Introduction

Shock tube apparatuses are often utilized for the investigation of high-temperature gasdynamics, and thermodynamic- and transport-properties. Hot stagnant ionized gases behind reflected shocks at the end wall of a shock tube have been used for experimental studies of the thermal conductivity [1], the heat transfer rate on the end wall [2], the ionization relaxation time [3] and the development of the end wall boundary layer [4]. Therefore, it is important to elucidate the situation in the reflected-shock flowfields. Several experimental investigations have indicated that these gas regions are complicated due to the interactions between ionization relaxation processes and reflected shocks. Smith [3] made measurements of the pressure-history at the end wall of a shock tube. He proposed a distance-time diagram of the reflected-shock flowfield in ionizing xenon, assuming simple models, in order to explain his experimental results. Kuiper and Bershader [1, 5] visualized the flowfields behind reflected shocks in ionizing argon by use of streak interferometry.

Numerical calculations of reflected-shock flowfields in relaxing gases have been performed for vibrational- [6] and dissociative-gases [7, 8]. But, to our knowledge, no numerical calculation has been carried out of the reflection processes in an ionizing gas in which more drastic changes occur than in chemically reacting gases. The present paper deals with numerical calculations on reflected-shock flowfields in ionizing argon gases. A finite difference method is employed to solve the time-dependent, one-dimensional inviscid flow problems for ionizing gases.

There are several phenomena affecting the reflected-shock flowfields, beside ionization relaxation processes. Briefly, we shall refer to these effects in the following. The unsteady thermal boundary layer forms on the end wall as a result of wall cooling. It gives rise to a negative displacement and reduces the reflected shock [9]. As is well-known, the side-wall boundary layer developed behind an incident shock bifurcates reflected shocks in a polyatomic gas, but not in a monatomic gas. However the bifurcation of reflected shock in ionizing argon was reported to result from the onset of ionization behind the incident shock [1, 5]. The radiation cooling, after ionization equilibration, also reduces the enthalpy of the ionized gas [1].

The above-mentioned phenomena provide their own problems to be studied. In the present paper, the effect of ionization relaxation processes on a reflected-shock flowfield is investigated in detail.

2. Numerical Analysis

2.1. Basic Equations

A schematic distance-time diagram is shown in Fig. 1, where x is the distance from the end wall of a shock tube and t is the time after reflection of an incident shock. The basic equations used in the present study are time-dependent one-dimensional conservation equations for ionized and thermally nonequilibrium inviscid gases:

$$\frac{\partial \varrho}{\partial t} + \frac{\partial (\varrho u)}{\partial x} = 0 , \tag{1}$$

$$\frac{\partial (\varrho u)}{\partial t} + \frac{\partial (\varrho u^2 + p)}{\partial x} = 0 , \tag{2}$$

Reprint requests to Prof. Dr. T. Akamatsu, Department of Mechanical Engineering, Kyoto University, *Kyoto 606*, Japan.

$$\frac{\partial}{\partial t}\left[\varrho\left(e+\frac{u^2}{2}\right)\right]+\frac{\partial}{\partial x}\left[\varrho u\left(e+\frac{u^2}{2}+\frac{p}{\varrho}\right)\right]=0 \quad (3)$$

where ϱ, u, p and e are the density, the velocity, the pressure and the energy. The equations of state for ionized monatomic gases are

$$p=\varrho(k/m_{\mathrm{h}})(T+c\,T_{\mathrm{e}})\,, \quad (4)$$

$$e=3\,p/2\,\varrho+c(E_{\mathrm{I}}/m_{\mathrm{h}}) \quad (5)$$

where T, T_e and c are the temperature of heavy particle gas, the electron temperature and the degree of ionization respectively, and k, m_h and E_{I} are the Boltzmann constant, the mass of a heavy particle and the ionization energy.

The electron conservation equation [10] is

$$\partial n_{\mathrm{e}}/\partial t+\partial(n_{\mathrm{e}}u)/\partial x=\dot{n}_{\mathrm{e}} \quad (6)$$

where n_e is the number density of electron and $\dot{n}_{\mathrm{e}}$ is the electron production rate. Equation (6) can be written in term of the degree of ionization as follows

$$\partial(\varrho c)/\partial t+\partial(\varrho c u)/\partial x=\varrho\dot{c} \quad (7)$$

where $\dot{c}$ is the production rate of the ionization degree.

The energy conservation equation of electron [10] is

$$\frac{\partial}{\partial t}\left(\frac{3}{2}n_{\mathrm{e}}kT_{\mathrm{e}}\right)+\frac{\partial}{\partial x}\left(\frac{3}{2}n_{\mathrm{e}}kT_{\mathrm{e}}u\right)+n_{\mathrm{e}}kT_{\mathrm{e}}\frac{\partial u}{\partial x}$$
$$=3\frac{m_{\mathrm{e}}}{m_{\mathrm{h}}}n_{\mathrm{e}}k(T-T_{\mathrm{e}})\nu_{\mathrm{eh}}-E_{\mathrm{I}}(\dot{n}_{\mathrm{e}})_{\mathrm{e}} \quad (8)$$

where m_e is the mass of an electron, ν_{eh} is the collision frequency between electron and heavy particles, and $(\dot{n}_{\mathrm{e}})_{\mathrm{e}}$ is the electron production rate due to atom-electron inelastic collisions. It is convenient for the numerical analysis to assume the electron gas in a local steady state: each term on the left-hand side of Eq. (8) is much smaller than either of the terms on the right-hand side. Then, the differential equation (8) reduces to such an algebraic equation as

$$T-T_{\mathrm{e}}=\frac{1}{3}\frac{\dot{c}_{\mathrm{e}}/c}{(m_{\mathrm{e}}/m_{\mathrm{h}})\nu_{\mathrm{eh}}}T_{\mathrm{ion}} \quad (9)$$

where $T_{\mathrm{ion}}=E_{\mathrm{I}}/k$ is the characteristic temperature of ionization. The local steady state approximation is known to be valid in almost all the part of the relaxation region except the ionization initiation zone immediately behind an incident shock [11].

The surface of the shock tube end wall located at $x=0$, is assumed to be impermeable and thermally insulated. This condition means that two identical shocks collide each other at the symmetric plane ($x=0$). After all, the differential equations (1), (2), (3) and (6) are to be solved with the algebraic relations of (4), (5) and (9). The initial conditions can be given by the profiles of ionization relaxation behind the incident shock propagating into the initial stationary region.

2.2. Ionization Production Rates and Collision Frequencies

In this section, we shall write down the formulas of ionization production rates and collision frequencies for argon plasma given by Hoffert and Lien [11].

The ionization reaction consists of two processes. One is the production due to atom-atom inelastic collisions:

$$\dot{c}_{\mathrm{a}}=(1-c)\left(\frac{\varrho}{m_{\mathrm{h}}}\right)^2 k_{\mathrm{ra}}(T)\frac{c_{eq}^2(T)-c^2}{1-c_{eq}^2(T)}\,. \quad (10)$$

The other is the production due to electron-atom inelastic collisions:

$$\dot{c}_{\mathrm{e}}=c\left(\frac{\varrho}{m_{\mathrm{h}}}\right)^2 k_{\mathrm{re}}(T_{\mathrm{e}})\frac{c_{eq}^2(T_{\mathrm{e}})-c^2}{1-c_{eq}^2(T_{\mathrm{e}})}\,. \quad (11)$$

Therefore, the net rate of the degree of ionization is

$$\dot{c}=\dot{c}_{\mathrm{a}}+\dot{c}_{\mathrm{e}}\,. \quad (12)$$

The equilibrium degrees of ionization are written as

$$c_{\mathrm{eq}}(T_{\mathrm{M}})=\left[1+\frac{(1+c)}{m_{\mathrm{h}}K_{\mathrm{eq}}(T_{\mathrm{M}})}\right]^{-1/2} \quad (13)$$

where $K_{\mathrm{eq}}(T_{\mathrm{M}})$ is the equilibrium constant ($T_{\mathrm{M}}=T$ or T_{e}):

$$K_{\mathrm{eq}}(T_{\mathrm{M}})=\frac{2Z_{\mathrm{i}}}{Z_{\mathrm{a}}}\left(\frac{2\pi m_{\mathrm{e}}kT_{\mathrm{M}}}{h^2}\right)^{3/2}\exp\left\{-\frac{T_{\mathrm{ion}}}{T_{\mathrm{M}}}\right\} \quad (14)$$

and Z_i/Z_a is the ratio of the electronic partition functions which can be approximated to be 6 for argon. The rate constants of argon [12, 13] used in the present numerical calculations are

$$k_{\mathrm{ra}}(T)=5.80\cdot10^{-37}\cdot\left(\frac{T_{\mathrm{A_1}}}{T}+2\right)$$
$$\cdot\exp\left(\frac{T_{\mathrm{ion}}-T_{\mathrm{A_1}}}{T}\right),\left(\frac{\mathrm{cm}^6}{\mathrm{s}}\right) \quad (15)$$

$$k_{re}(T_e) = 1.29 \cdot 10^{-32} \cdot \left(\frac{T_{A_1}}{T_e} + 2\right) \cdot \exp\left(\frac{T_{ion} - T_{A_1}}{T_e}\right), \left(\frac{cm^6}{s}\right) \quad (16)$$

where the characteristic temperatures of ionization and excitation are $T_{ion} = 183100\ ^\circ K$ and $T_{A1} = 135300\ ^\circ K$.

The elastic collision frequency between electrons and heavy particles ν_{eh} is the sum of electron-ion collision frequency ν_{ei} and electron-atom collision frequency ν_{ea}:

$$\nu_{eh} = \nu_{ei} + \nu_{ea}, \quad (17)$$

$$\nu_{ei} = \frac{c\varrho}{m_h}\left(\frac{8kT_e}{m_e}\right)^{1/2} Q_{ei}, \quad (18)$$

$$\nu_{ea} = \frac{(1-c)\varrho}{m_h}\left(\frac{8kT_e}{m_e}\right)^{1/2} Q_{ea}. \quad (19)$$

The elastic collision cross-section between electrons and atoms [14] adopted in the present numerical calculations is

$$Q_{ea} = \begin{cases} (-0.35 + 0.775 \cdot 10^{-4} \cdot T_e) \cdot 10^{-16}, (cm^2) \\ \quad 10^4\ ^\circ K < T_e < 5 \cdot 10^4\ ^\circ K; \\ (0.39 - 0.551 \cdot 10^{-4} \cdot T_e + 0.595 \cdot 10^{-8} \cdot T_e^2) \\ \cdot 10^{-16}, (cm^2) \\ \quad T_e < 10^4\ ^\circ K \end{cases} \quad (20)$$

and the elastic collision cross-section for electrons and ions [10] can be expressed as

$$Q_{ei} = \frac{2\pi e^4}{9k^2 T_e^2} \ln\left(\frac{9k^3 T_e^3}{4\pi e^6 n_e}\right). \quad (21)$$

2.3. Finite Difference Equations

As the aforementioned differential equations are of the form;

$$\partial U/\partial t + \partial F(U)/\partial x = G, \quad (22)$$

we can apply the two-step Lax-Wendroff scheme [15] which is written as follows:

$$\begin{aligned} U_j^{n+1} &= U_j^n - \frac{\lambda}{2}\{\tfrac{1}{2}(F_{j+1}^n - F_{j-1}^n) + (\tilde{F}_{j+\frac{1}{2}}^{n+1} - \tilde{F}_{j-\frac{1}{2}}^{n+1})\} + G_j^{n+\frac{1}{2}} \Delta t, \\ G_j^{n+\frac{1}{2}} &= G[\tfrac{1}{4}(2U_j^n + \tilde{U}_{j+\frac{1}{2}}^{n+1} + \tilde{U}_{j-\frac{1}{2}}^{n+1})], \\ \tilde{F}_{j+\frac{1}{2}}^{n+1} &= F(\tilde{U}_{j+\frac{1}{2}}^{n+1}), \\ \tilde{U}_{j+\frac{1}{2}}^{n+1} &= \tfrac{1}{2}(U_{j+1}^n + U_j^n) - \lambda(F_{j+1}^n - F_j^n) + G_{j+\frac{1}{2}}^n \Delta t, \\ G_{j+\frac{1}{2}}^n &= G[\tfrac{1}{2}(U_{j+1}^n + U_j^n)] \end{aligned} \quad (23)$$

where the subscripts j and n refer to the grid points of x- and t-coordinates, Δx and Δt are the stepsizes of them, and $\lambda = \Delta t/\Delta x$ which must satisfy the Courant-Friedrich-Lewy condition [16]:

$$\Delta t/\Delta x \leqq 1/\mathrm{Max}(a + |u|) \quad (24)$$

where a is the speed of sound given by

$$a^2 = \frac{5}{3}\frac{p}{\varrho}. \quad (25)$$

2.4. Boundary Conditions and Initial Conditions

The wall is located at the grid point $j = 0$ corresponding to $x = 0$. As the condition of symmetricity is hold at $j = 0$, U_j^n at the grid point $j = -1$ is determined in the following way:

$$\begin{aligned} &u_{-1}^n = -u_1^n, \quad \varrho_{-1}^n = \varrho_1^n, \quad p_{-1}^n = p_1^n, \\ &e_{-1}^n = e_1^n, \quad c_{-1}^n = c_1^n. \end{aligned} \quad (26)$$

Then, U_j^{n+1} at $j = 0$ is evaluated from U_j^n at $j = -1$, 0 and 1 by Equation (23).

In order to shorten computation time, the computation domain is restricted within the zigzag area as shown in Figure 1. The conditions on the zigzag boundary are evaluated by the relation of $U(x, t+\xi) = U(x + U_s\xi, t)$.

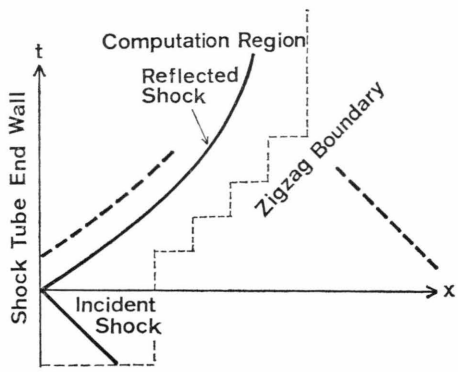

Fig. 1. Schematic distance-time diagram for shock reflection on the end wall of a shock tube.

3. Results and Discussions

3.1. Results of Numerical Calculations

Numerical calculations have been conducted for three cases summarized in Table 1, which are obtainable by a conventional free-piston shock-tube apparatus. The distance-time diagrams for these

Table 1. Conditions of numerical calculations: Incident shock Mach number, initial pressure, shock speed and step-sizes of finite difference scheme.

Case	M_s	p_1	U_s	Δx	Δt
1	16	1 torr	5.16 km/s	0.1453 mm	0.01935 μs
2	14	3	4.52	0.1001	0.01519
3	12	5	3.87	0.1345	0.02372

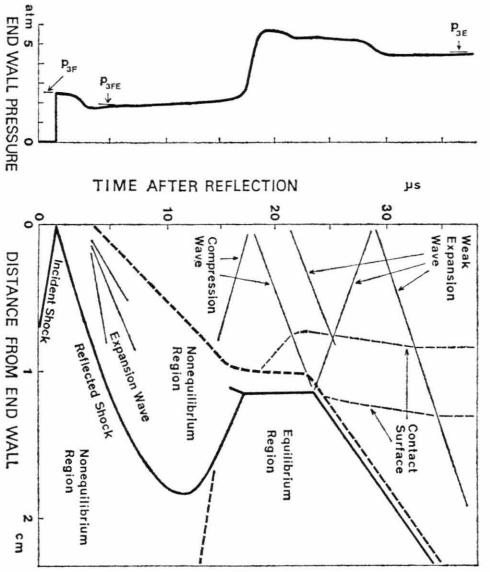

Fig. 2. Distance-time diagram of shock reflection processes for Case 1: $M_s = 16$ and $p_1 = 1$ torr.

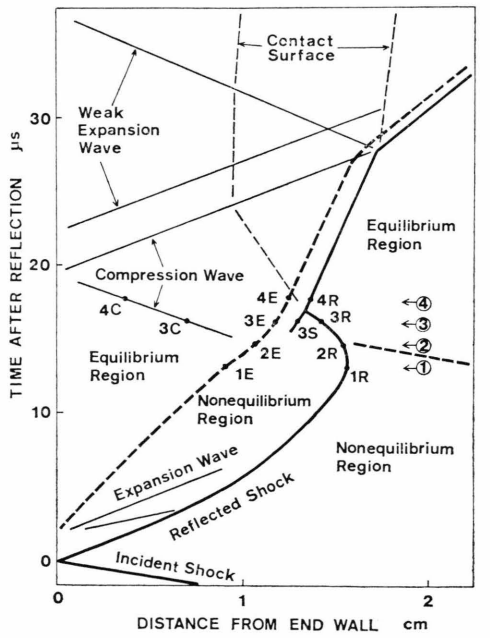

Fig. 3. Distance-time diagram of shock reflection processes for Case 2: $M_s = 14$ and $p_1 = 3$ torr.

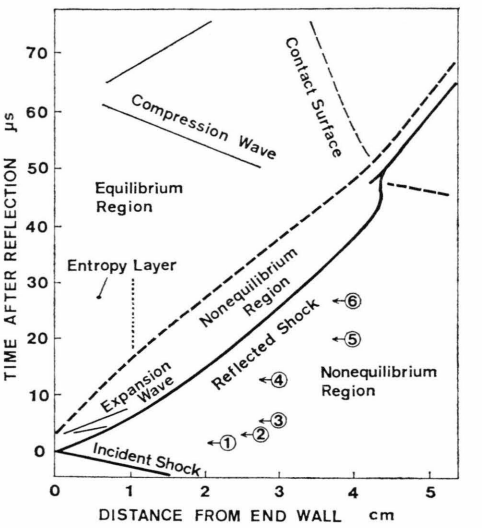

Fig. 4. Distance-time diagram of shock reflection processes for Case 3: $M_s = 12$ and $p_1 = 5$ torr.

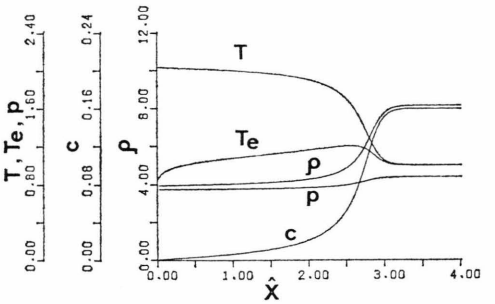

Fig. 5. Nondimensional plots of the flowfield behind the incident shock for Case 1, characteristic values are $x_0 = 2.91$ cm, $\varrho_0 = 2.13 \cdot 10^{-6}$ g/cm^3, $T_0 = 11913$ °K, $u_0 = 5.16$ km/s and $p_0 = 0.561$ atm.

three cases are shown in Figures 2, 3 and 4. We shall explain the reflection processes mainly referring to Figure 2. Figure 5 shows the profiles of the incident-shock flowfield which consists of three main regions: the frozen region, the ionizing region and the equilibrium region. For a short time after the reflection of the incident shock, the shocked gas is in a frozen state. In the meantime, the ionization reaction proceeds in the frozen region and the reflected shock begins to move rather slowly. Then, the sudden onset of equilibration beginning at the end wall, the temperature falls down and the density increases in the equilibrium region adjacent to the end wall because the ionization reaction removes the ionization energy from the kinetic energy. Consequently,

expansion waves propagate away from the end wall and weaken the reflected shock. Figure 6 shows the computer plots of the reflected-shock flowfields at $t=5.22\ \mu$s: the reflected shock arrives at $x=1.22$ cm ($\hat{x}=0.42$), the gas is in an equilibrium state near the end wall, $x=0\sim0.15$ cm ($\hat{x}=0\sim0.05$), and the expansion wave has the minimum pressure at $x=0.55$ cm ($\hat{x}=0.19$):

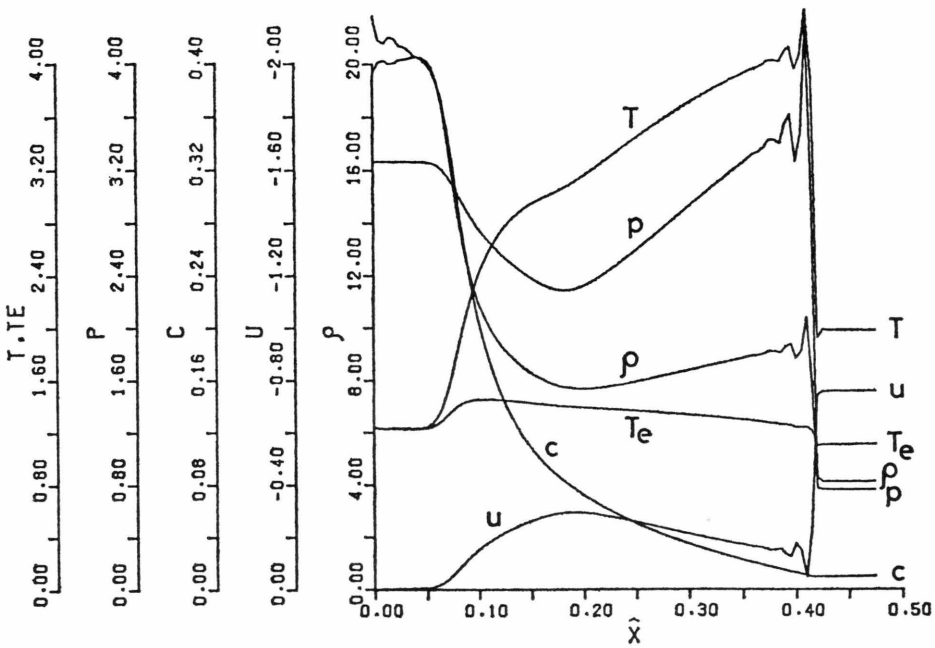

Fig. 6. Nondimensional plots of the flowfield behind the reflected shock at 5.22 μs after reflection for Case 1.

The pressure history at the end wall is shown next to the diagram in Fig. 2, where p_{3F}, p_{3FE} and p_{3E} are calculated assuming simple reflected-shock relations: the subscript 3F means a reflected shock in a perfect gas and the subscripts 3FE and 3E refer to equilibrium reflected shocks moving to frozen and equilibrium incident gas flow, respectively. Immediately after reflection, the end wall pressure rises to p_{3F}, and then it drops at the onset of equilibration ($t=2.9\ \mu$s), being followed by the slow recovery of pressure to p_{3FE}.

The reflected shock is attenuated by the overtaking expansion waves as well as by the increase in the gas density in front of the reflected shock. However, in Case 3, these effects are isolated because the relaxation time of the incident shock is much longer than that of the reflected shock as shown in Figure 4. Hence, the influence of expansion waves on a reflected shock can be considered separately.

Figure 4 indicates that the reflected shock travels away from the end wall at the frozen speed immediately after reflection and subsequently it is decelerated to the equilibrium speed. This transient reflection process forms the nonuniform region near the end wall which is called as an entropy layer in vibrational [6] or dissociative gases [7, 8]. The profiles of the electron number density of the reflected-shock flowfield are shown in Fig. 7 for several discrete times marked in Figure 4. The electron number density n_{eFE} in Fig. 7 is calculated assuming the equilibrium reflected shock and the frozen incident shock. The electron number density adjacent to the wall exceeds the equilibrium value of n_{eFE}, because these gas particles are processed by a stronger frozen reflected shock than the equilibrium reflected shock. In the almost uniform region beyond the entropy layer ($x\geqq1.1$ cm), the number density of electrons attains slightly above the equilibrium value due to the influence of the ionization relaxation behind the incident shock.

As the gas in front of the reflected shock relaxes into equilibrium and its density increases, the reflected shock is decelerated and then, it goes back towards the end wall ($t=15\ \mu$s, in Figure 2). We shall discuss how the reflected shock propagating back to the end wall interacts with the equilibrium

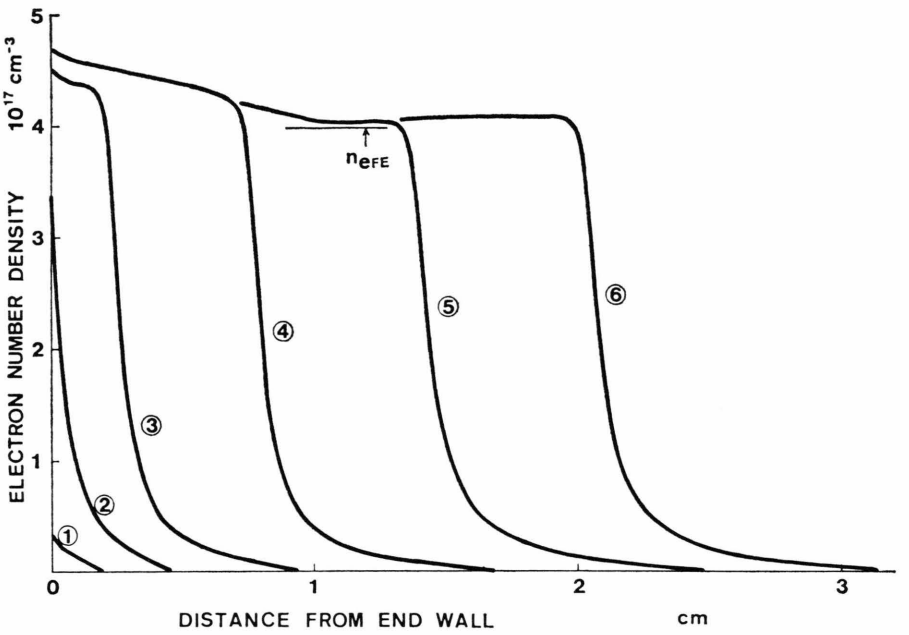

Fig. 7. Profiles of the number density of electrons at discrete times after reflection: (1) 1.07 μs, (2) 2.49 μs, (3) 5.34 μs, (4) 12.45 μs, (5) 19.57 μs, (6) 26.68 μs.

region behind it, referring to Figure 3. Typical profiles of the flowfield marked with 1, 2, 3 and 4 in Fig. 3 are shown in Figure 8. The reflected shock is denoted by 1R, 2R, etc. and the onset of equilibration is denoted by 1E, 2E, etc. The profile 1 shows the flowfield that the reflected shock almost ceases moving and the upstream gas is still in nonequilibrium. In the profile 2, the retiring shock weakening, the pressure and the temperature of the nonequilibrium region behind it are reduced. But the pressure in the neighborhood of 2E point grows high and the temperature of the relaxation region becomes higher at the last stage of relaxation because of the gas moving against the steep pressure gradient. In the profile 3, from the high-pressure zone (3E) between the equilibrium region and the nonequilibrium region, a compression wave (3C, 4C) is generated and propagates towards the end wall. Simultaneously a shock (3S) is also produced moving to the reflected shock. Colliding of this newly generated shock with the reflected shock gives rise to a contact surface where the density and the degree of ionization are discontinuous but the temperature is almost continuous.

The end-wall pressure history in Fig. 2 shows that there is an abrupt pressure increase at $t=$

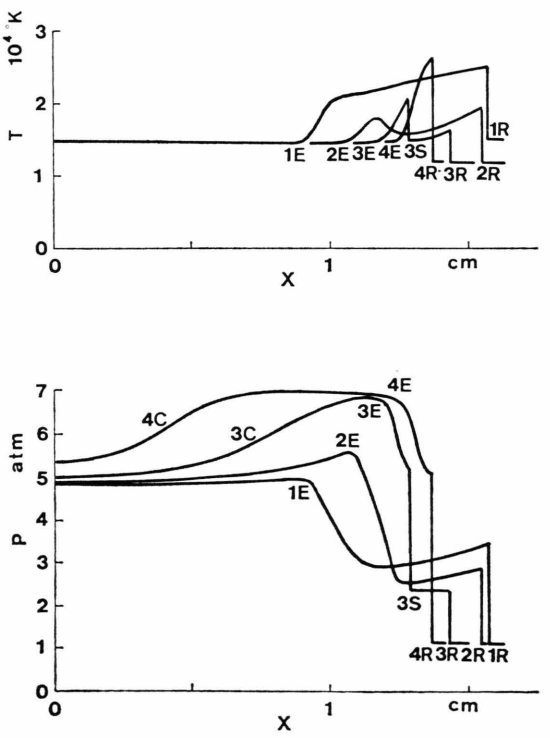

Fig. 8. Profiles of the pressure and the temperature of heavy particles for Case 2: Numbers 1, 2, 3 and 4 refer to 13.14 μs, 14.66 μs, 16.18 μs and 17.70 μs after reflection, respectively.

17.8 μs. It is due to the reflection of the compression wave caused by the aformentioned interaction. Then, weak expansion waves are caused due to the secondary ionization relaxation ($t = 21.6\ \mu$s) and follow after the reflected compression wave. The reflected compression wave catching up with the reflected shock strengthens it and propagates back as a weak expansion wave. At the same time, another contact surface is generated, where the density and the degree of ionization are again discontinuous but the temperature is almost continuous. The end-

by use of time-resolved Mach-Zehnder interferometry, and made the distance-time diagrams for the case of the initial pressure of $p_1 = 5$ torr and the incident shock Mach numbers of $Ms = 11.4$ and $Ms = 12.7$. The qualitative agreement with our distance-time diagram of Case 3 (Fig. 4) is good, while the quantitative comparison is inadequate because the relaxation times of the incident shocks in his experiments are shorter than those of our numerical results. Generally, in the experiments, the ionization relaxation time behind an incident shock is shorten-

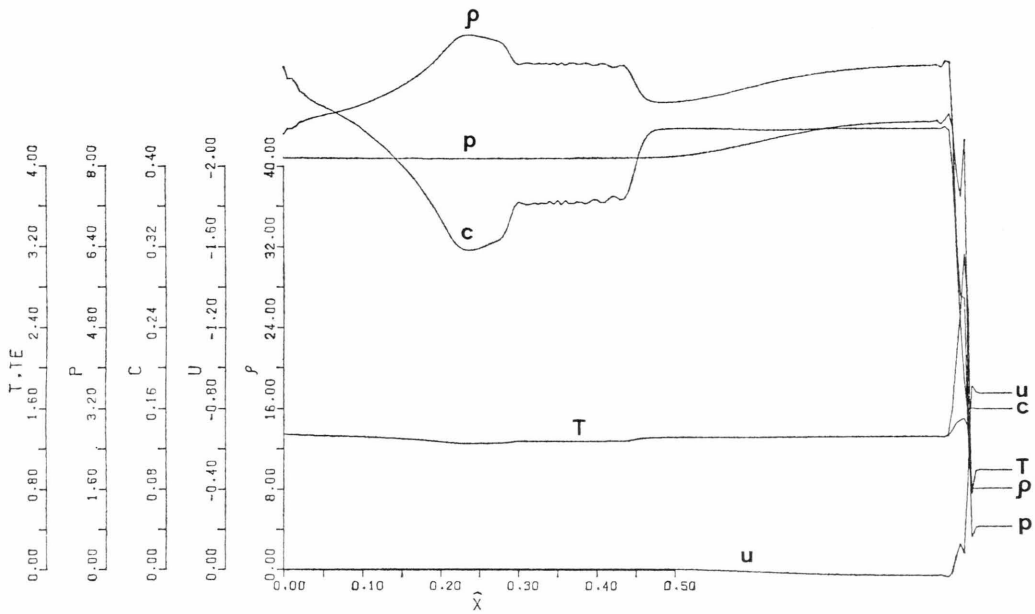

Fig. 9. Nondimensional plots of the flowfield behind the reflected shock at 36.18 μs after reflection for Case 1.

wall pressure decreases due to this expansion wave and then increases slightly to the equilibrium value of p_{3E}.

Figure 9 shows the computer plots of the hot stagnant region where the reflected shock passed through ($t = 36.18\ \mu$s, in Figure 2). The pressure- and temperature-profiles are straightforward there, but the profiles of the density and of the degree of ionization are not so simple due to the interactions between ionization relaxation processes and waves.

3.2. *Comparisons with Experiments and Discussions*

Kuiper [1, 5] obtained the measurements of the time history of the electron number density and the mass density behind the reflected shock in ionizing argon

ed by several effects such as an impurity of test gases [17], an incident side-wall boundary layer [18] and so on. The ionization relaxation times in our calculations coincide with the experimental relaxation times by Wong and Bershader [19]. It is also shown by Kuiper [1] that the measured electron number density at the edge of the boundary layer on the end wall is larger than the theoretical equilibrium one: for example, $n_e = 4.55 \cdot 10^{17}\ \mathrm{cm}^{-3}$ for the condition of $p_1 = 5$ torr and $Ms = 12$, and its equilibrium value is $n_{eFE} = 3.98 \cdot 10^{17}\ \mathrm{cm}^{-3}$. Our results of Fig. 7 are comparable.

Smith [3] made the measurements of the pressure history in ionizing xenon with the fast-rise pressure gauge mounted in the end wall of the shock tube. The present results of the end-wall pressure history

shown in Fig. 2 gives a similar profile to his experimental one.

We have neglected the existance of Ar^{++}-ions in our numerical calculations. According to JPL Technical Report [20], the concentration of Ar^{++}-ions behind the equilibrium reflected shock is less than $1 \cdot 10^{-3}\%$ in such a condition as in Table 1: for example, the number densities of Ar-atoms, Ar^{+}-ions and Ar^{++}-ions behind the equilibrium reflected shock are $9.2 \cdot 10^{17}\,cm^{-3}$, $6.8 \cdot 10^{17}\,cm^{-3}$ and $2.5 \cdot 10^{13}\,cm^{-3}$ respectively, for the condition of the incident shock velocity $U_s = 5.22$ Km/s, the initial pressure $p_1 = 1$ torr and the initial temperature $T_1 = 300\,^{\circ}K$. Hence our dismissal of Ar^{++}-ions is valid.

In the present study, we have employed the formulas of ionization rates and collision cross-sections used by Hoffert and Lien [11]. It should be noted that the collision cross-section between electrons and atoms Q_{ea} discussed by Devoto [21] is several times larger and the ionization rate due to atom-atom inelastic collisions k_{fa} determined by McLaren and Hobson [22] is several factors smaller than those used here.

4. Conclusion

Numerical calculations of the ionizing shock reflection at a closed end of a shock tube have been performed by use of the two-step Lax-Wendroff scheme. Some interesting phenomena and complicated flowfields have been found out which occur due to the interaction between ionization relaxation processes and reflected shocks. The effects of radiation cooling and the interaction between a reflected shock and an incident side-wall boundary layer might have to be taken into consideration hereafter. The present finite difference procedure is applicable straightforward to solve the present problems including the radiation energy loss.

[1] R. A. Kuiper, Proc. 7th Int. Shock Tube Sym., Canada, 721 [1969].
[2] M. Camac and R. M. Feinberg, J. Fluid Mech. **21 4,** 673 [1965].
[3] J. A. Smith, Phys. Fluid **11,** 2150 [1968].
[4] A. C. B. Hutten Mansfeld, E. J. M. van Heesch, M. E. H. van Dongen, and G. Vossers, Proc. 12th Int. Conf. Phen. Ion. Gases, North-Holland, 391 [1975].
[5] R. A. Kuiper and D. Bershader, AIAA J. **7,** 777 [1969].
[6] N. H. Johannesen, G. A. Bird, and H. K. Zienkiewicz, J. Fluid Mech. **30 1,** 721 [1971].
[7] L. L. Presley and R. K. Hanson, AIAA J. **7,** 2267 [1969].
[8] M. Matsushita and T. Akamatsu, Mem. Faculty Eng. Kyoto Univ. **34 1** [1977].
[9] J. A. Fay and N. H. Kemp, J. Fluid Mech. **21 4,** 659 [1965].
[10] G. W. Sutton and A. Sherman, Engineering Magnetohydrodynamics, McGraw-Hill Inc., New York 1965.
[11] M. I. Hoffert and H. Lien, Phys. Fluids **10,** 1769 [1967].
[12] A. J. Kelly, J. Chem. Phys. **45,** 1723 [1966].
[13] H. Petschek and S. Byron, Ann. Phys. New York **1,** 270 [1957].
[14] M. Y. Jaffrin, Phys. Fluids **8,** 606 [1965].
[15] E. L. Rubin and S. Z. Burstein, J. Comp. Phys. **2,** 178 [1967].
[16] R. D. Richtmyer and K. W. Morton, Difference Methods for Initial-Value Problems, 2nd ed., Interscience Publishers 1967.
[17] G. Kamimoto and K. Teshima, Dept. Aero. Eng., Kyoto Univ. C. P. 32 [1972].
[18] Y. Enomoto, J. Phys. Soc. Japan **35 4,** 1228 [1973].
[19] H. Wong and D. Bershader, J. Fluid Mech. **26 3,** 459 [1966].
[20] W. A. Menard and T. E. Horton, JPL Tech. Rep. 32-1408 vol. III, Shock Tube Thermochemistry Tables for High-Temperature Gases [1970].
[21] R. S. Devoto, Phys. Fluids **10,** 354 [1967]; Phys. Fluids **16,** 616 [1973].
[22] T. I. McLaren and R. M. Hobson, Phys. Fluids **9,** 2162 [1968].